The DØ Detector at TeV33

The DØ Collaboration
Draft Version 2

July 13, 1997

1 Introduction

An upgraded Fermilab Tevatron (TeV33), capable of delivering to tape integrated luminosities of order 30 fb^{-1}, offers a compelling physics program [1]. The DØ experiment would expect to reconstruct more than 10,000 b tagged top decays, to measure the W mass to 20 MeV/c^2, to discover supersymmetry or rule it out over large fractions of the available parameter space, and to observe CP violation in b decays. We consider here the performance of the DØ detector in the TeV33 environment at luminosities up to 2×10^{33} cm^{-2}s^{-1}. We find that the detector will function well with substantial upgrades provided that the average number of interactions per crossing does not exceed 6 or 7. Luminosity leveling is clearly an important part of a plan to reach high luminosity.

We assume Run II will last until 2.0 fb^{-1} have been delivered, followed by roughly a half year shutdown for installation of our Run III detector. This detector must remain healthy for four years of higher luminosity running prior to significant LHC operations. We further assume that upgrade Equipment funding will be available starting in 2001 to finance the Run III upgrades.

In this paper, we detail the effects of high luminosity on the various parts of the DØ detector beginning with the calorimeter.

2 Calorimeter

The high luminosity projected for TeV33 substantially increases the average energy deposited during the DØ calorimeter's ≈ 400 ns integration time. This increase leads to two principle areas of concern: the effect of the increased underlying event energy on physics analyses and technical limitations on the calorimeter performance at high luminosity due to the calorimeter design. In this section, we report on studies of these effects within the context of the present upgrade calorimeter design. We also briefly mention studies of possible modifications to the present calorimeter design.

The average energy deposited in a calorimeter tower (0.1×0.1 in $\eta \times \phi$ space) due to minimum bias events was measured during Run I using zero bias triggers with calorimeter noise suppression (i.e. pedestal subtraction) turned off. Scaling to a luminosity of 10^{33} cm^{-2}s^{-1} with 108 bunches, minimum bias events will contribute an average transverse energy of ≈ 65 MeV for central EM towers and ≈ 20 MeV for central hadronic towers. For comparison, in Run I the central underlying event energy was dominated by the uranium noise contribution, which gave an average energy (not E_T) deposit of ≈ 5

MeV in a central EM tower and ≈ 9 MeV in a central hadronic tower. Thus, the underlying event at TeV33 is expected to be dominated by the minimum bias events accompanying the hard process.

It should be possible to subtract the average underlying event energy with good precision, but fluctuations about the average will add a noise contribution to the measurement of the transverse energy of electrons, photons, jets, and to missing E_T. Further work is needed to quantify the various noise contributions; nevertheless, it is probably reasonable to assume that the noise is $\approx 100\%$ of the mean energy deposited. In addition, we need to include the electronic noise contribution, which on average does not contribute to the underlying event energy.

The effect of underlying event noise is expected to have a minor impact on most of the DØ TeV33 physics program. The jet energy resolution will continue to be dominated by fragmentation and showering fluctuations. The precision of the top quark mass measurement is expected to be set by systematic errors in the jet energy scale and the Monte Carlo modeling of gluon radiation. A study of large missing E_T SUSY signatures [1] found that the rejection of QCD background events was not significantly affected by underlying event pile-up.

The physics measurement that will be most affected by underlying event noise is the precision measurement of the W mass. The effect of increased underlying event pile-up was studied for the TeV2000 report [2], with the conclusion that a W mass uncertainty of 30 MeV/c^2 was achievable with 10 fb^{-1}. The transverse mass resolution at high luminosity is dominated by the missing E_T resolution, with the contribution from underlying event noise becoming roughly equal to the intrinsic detector resolution at a luminosity of $\approx 2 \times 10^{32}$ cm^{-2}s^{-1} [3]. Further increases in luminosity are likely to degrade the transverse mass resolution such that the statistical accuracy is not improved by increasing the luminosity. Nevertheless, one would expect TeV33 to yield a factor of ≈ 10 improvement in the statistical error over our present Run I results. It is not clear that a comparable reduction in the systematic error can be achieved. An alternative technique for measuring the W mass is the ratio method, where W and Z events are analyzed in an identical manner by ignoring one of the electrons in $Z \rightarrow ee$ decay. This method has been applied to the DØ Run Ia sample, yielding a statistical error of 360 MeV for 13 pb^{-1}. The statistical error on the ratio method extrapolates to $\approx 10 - 20$ MeV for TeV33, with a potentially smaller systematic error than can be achieved from the transverse mass fits due to the reduced sensitivity to the modeling of the W production distributions [4].

As the luminosity is increased for TeV33, the DØ calorimeter performance will be affected by the increase in absorbed energy per unit time. While the DØ calorimeter is believed to be immune to radiation damage, the increase in particle flux leads to an increase in the ionization current flowing across the liquid argon gap. The high voltage supply is connected to the resistive coat at the outer edge of the calorimeter. The ionization current flowing across the gap produces a voltage drop across the resistive coat, decreasing the voltage across the liquid argon gap. Since the drift velocity of the ionized electrons in the argon depends on the electric field, a large voltage drop across the resistive coat will change the shape of the signal pulse and decrease the charge collection efficiency. The largest voltage drop occurs for the EM3 layer in the EC, which is located near the shower maximum and has the largest ionization current.

The voltage drop was calculated from the average energy per beam crossing deposited in the calorimeter. The data used was from zero bias runs taken with calorimeter noise suppression turned off. The ionization current is given by

$$I_0 = \frac{\bar{E} F_S e f}{2I} \tag{1}$$

where $\bar{E}$ is the average energy in a beam crossing, F_S is the sampling fraction, e is the electron charge,

f is the beam crossing frequency, and I is the ionization potential for argon. These results are shown in Fig. 1. Increasing the high voltage from 2.0 to 2.5 kV would probably lead to an acceptable gap voltage for EM3, although the changing drift velocity will affect the calorimeter energy response and likely require luminosity and pseudorapidity η dependent corrections. [We note that there is still a discrepancy between the voltage sag calculated using the energy deposited in the calorimeter and that calculated using the HV supply currents since the HV supply currents at low luminosities (less than 2.5×10^{29} cm^{-2} s^{-1}) changed by nearly a factor of two during Run I and were not ϕ symmetric. The calculation based on measurements of the deposited energies is felt to be more reliable.]

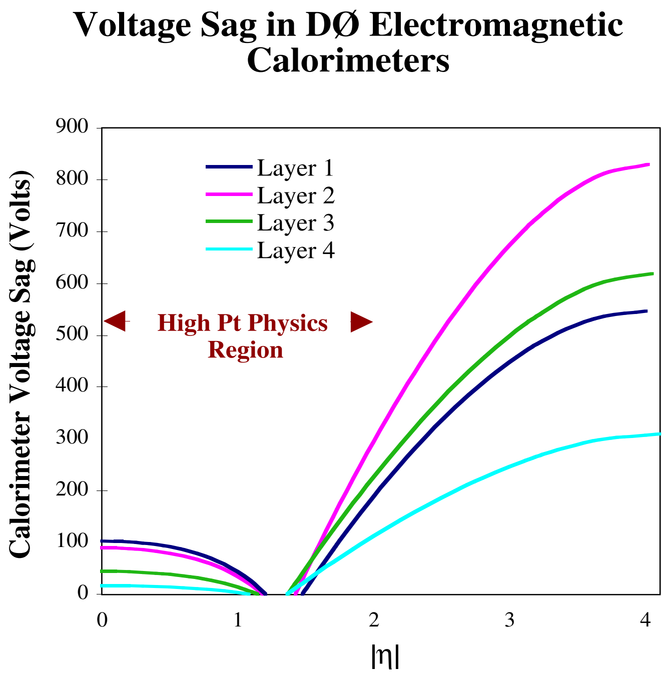

Figure 1: Voltage drop vs. $|\eta|$ determined from zero bias events.

Two modifications to the Run II calorimeter design have been considered: increasing the number of bunches to 146 and modifying the calorimeter to speed up charge collection. By eliminating two of the abort gaps, the number of bunches can be increased from 108 to 146. For a given luminosity, this reduces the underlying event energy from minimum bias events by 26%, giving a small reduction in underlying event noise. Eliminating the abort gaps will require some modification to the calorimeter readout since there are insufficient capacitors on the SCA's to hold all 146 samples. This modification may result in small pedestal shifts that will need to be corrected for when the readout "wraps" around from the last capacitor in the SCA to the first. In addition, there will be an increase in the electronic noise due to the longer time between baseline samples. The impact of the increased noise needs to be quantified.

There has also been an investigation of possible calorimeter modifications that would increase the electron drift speed [5]. By increasing the drift speed, the integration time could be reduced, decreasing the number of crossings that the calorimeter integrates over. In addition to potentially major modifications of the DØ calorimeters, a substantial upgrade of the calorimeter electronics would also be required. There is concern that such changes may be beyond the limited scope of the DØ TeV33 upgrade.

In summary, the present DØ calorimeter appears to be capable of operating in the TeV33 environment. The increase in underlying event noise is mostly a concern for the precision W mass measurement. This measurement is expected to be limited by our understanding of systematic errors; recent work using the W/Z ratio method suggests that this method may be useful in reducing systematic errors. Voltage drops in the resistive coat will likely require an increase in the HV applied to some EC layers.

3 The Preshower Detectors

The DØ preshower detectors consist of a central detector [6] and two forward detectors [7]. They are designed to improve electron identifications in Run II. The detectors are composed of radiators and extruded scintillating triangular strips with embedded wavelength–shifting (WLS) fiber readout. Scintillating light produced by charged particles from either collisions or showers in the radiators is collected by the WLS fibers and piped through clear fibers to the visible light photon counters (VLPC) outside the calorimeter. The central detector covers the pseudorapidity range $|\eta| < 1.1$ and the forward detectors cover the range $1.4 < |\eta| < 2.5$. An online electron trigger is realized by requiring a large pulse in the preshower detectors matched with a track in the fiber tracker for the central detector and in the scintillating strips in front of the converter for the forward detectors.

In the following sections, we discuss potential problems such as occupancy, rate and radiation dose in operating the preshower detectors in Run III.

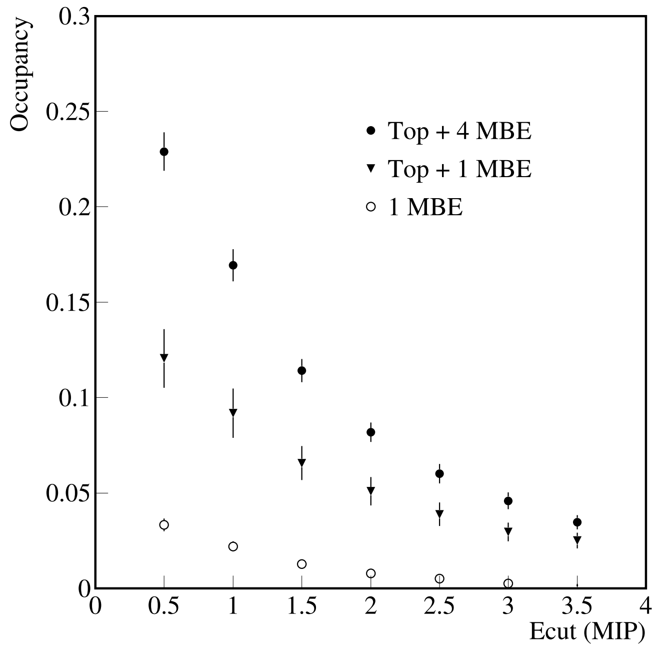

Figure 2: The expected occupancy as a function of the energy deposition in the axial strips of the central detector for minimum bias events and for $t\bar{t}$ events with one and four minimum bias events overlapped.

3.1 Occupancy

At a luminosity of $\mathcal{L} = 1 \times 10^{33}$ cm^{-2}s^{-1} with a 132 ns bunch spacing, on average there will be about 7 interactions per crossing. Figure 2 shows the expected occupancies as functions of the energy deposition for the axial strips of the Run II central preshower detector for minimum bias (MB) events and $t\bar{t}$ events with four minimum bias events overlapped. Here the occupancy is defined as the ratio between the number of strips with hits with energies above threshold and the total number of strips. The occupancies for the stereo strips are expected to be slightly worse. The occupancies at 1 MIP threshold are about 2% for one MB event and about 17% for a typical $t\bar{t}$ event overlapped with four MB events, where the unit MIP is defined as the most probable energy deposition in the layer by a muon. Assuming the occupancy increases linearly with the number of MB events, about 23% of the strips will be hit for a $t\bar{t}$ event at a luminosity $\mathcal{L} = 1 \times 10^{33}$ cm^{-2} s^{-1}. Even with a 3 MIP threshold, the occupancy will be around 9%. This high occupancy level will probably affect the online electron trigger more than offline electron identification. To fully understand its impact, detailed online and offline simulations are needed.

3.2 The Rate Issue

The high rate expected for the high luminosity is a concern for the VLPC photodetector. The issue of the gain and quantum efficiency (QE) of the VLPC at high rate has been studied in detail. The single photoelectron (PE) rate is approximately given by

$$R = 2 \cdot \mathcal{L}\sigma \cdot occ \cdot y,$$

where $\mathcal{L}$ is the instantaneous luminosity, σ is the total cross section, occ is the occupancy with a 1 MIP threshold and y is the photoelectron yield for a 1 MIP energy deposition. A factor of two is included to take into account the yield for the hits below threshold. Although failing the threshold, these hits still contribute to the single PE rate. For the Run II design luminosity of $\mathcal{L} = 2 \times 10^{32}$ cm^{-2} s^{-1}, the single PE rate is about 8 MHz assuming $\sigma = 50$ mb, $o = 2\%$ and $y = 20$ PE/MIP [1] for axial strips of the central detector. At a Run III luminosity of $\mathcal{L} = 1 \times 10^{33}$ cm^{-2} s^{-1}, the single PE rate is 40 MHz, five times higher. However, it should be noted that a yield of 20 PE/MIP has a considerable safety margin for achieving the required performance of a preshower detector. Halving the yield is not expected to significantly degrade the performance of the detector. Nominally, a 20 MHz rate capability of the VLPC's is needed. Including a factor of two for the uncertainty, we conclude that a 40 MHz VLPC rate capability should be sufficient for the Run III application. Recent studies of the VLPC characteristics seem to indicate that the gain and QE of the new VLPC's show little dependence on the rate implying the rate is not a problem.

3.3 Radiation Damage

Albedo neutrons from the calorimeter, and charged and neutral hadrons from $p\bar{p}$ interactions are the main sources of radiation in the preshower detector.

The central tracking volume is filled with albedo neutrons which are homogeneously distributed in $r_\perp$, the distance perpendicular to the beams. The logarithmic energy spectrum peaks roughly around 1 MeV. The estimated neutron flux density is $\phi_n = 1.2 \times 10^4$ cm^{-2}s^{-1} at a luminosity of

[1] This is the expected photoelectron yield based on the cosmic–ray test, see [8] for details.

$\mathcal{L} = 10^{32}$ cm^{-2}s^{-1}. Using a conversion factor of 1 neutron/cm^2 = 1.8×10^{-9} rad, the dose rate from neutrons is given by $\frac{dD_n}{dt} = 2.2 \times 10^{-5}(\mathcal{L}/10^{32}\text{cm}^{-2}\text{s}^{-1})$ rad/s.

Assuming a minimum bias event cross section 50 mb and 4 charged particles per unit of pseudorapidity, the charged particle flux at a radius is $\phi_{\pm} = 3.2 \times 10^6/(r_\perp/1\text{cm})^2$ cm^{-2}s^{-1}. Taking into account a factor of two for low p_T loopers, the dose rate from the charged particles is given by $\frac{dD_\pm}{dt} = \phi_\pm \times \frac{1}{\rho}\frac{dE}{dx} = \frac{0.2}{(r_\perp/1\text{ cm})^2}$ rad/s.

Most neutral hadrons are π^0's and have an average p_T of 0.5 MeV. From isospin symmetry, the π^0 flux is expected to be half of the flux for charged particles. Assuming each photon from π^0 decay cascades to 4 electrons in the solenoid and the lead, the expected dose rate from neutral hadrons is $\frac{dD_0}{dt} = 4\phi_\pm(\frac{1}{\rho}\frac{dE}{dx}) = \frac{0.6}{(r_\perp/1\text{ cm})^2}$ rad/s.

Adding the rates from neutron, charged and neutral hadrons together, the total dose rate at $\mathcal{L} = 10^{32}$ cm^{-2}s^{-1} is $\frac{dD}{dt} = 2.2 \times 10^{-5} + \frac{0.8}{(r_\perp/1\text{ cm})^2}$ rad/s. The total radiation doses for the central and forward detectors are shown in Fig. 3 as functions of integrated luminosity. The detailed calculation can be found in Ref. [9]. The above calculation has been checked using fully simulated minimum bias events for the central detector. The numbers from the calculation and the simulation agree very well. The expected radiation level for an integrated luminosity of 30 fb^{-1} in Run III is 54 krad for the central preshower, 140 krad at $\eta = 2.0$ and about 500 krad at $\eta = 2.5$ for the forward preshower. The dose in the central detector is well below the level at which the scintillator or fibers are affected. However, the dose in the forward detectors is high. The scintillator and fibers in the region $|\eta| > 2.0$ will suffer severe radiation damage and therefore the performance of the forward preshower detectors will degrade significantly.

3.4 Preshower Summary

As discussed above, it appears that the central detector and part ($|\eta| < 2.0$) of the forward detectors can operate with the Run III luminosity of $\mathcal{L} = 1 \times 10^{33}$ cm^{-2}s^{-1}. The high pseudorapidity region ($|\eta| > 2.0$) of the forward detectors is expected to suffer significant radiation damage. However, since most of the high p_T electrons are in the central region ($|\eta| < 2.0$), high p_T physics is not expected to suffer even though radiation damage will reduce the response of the very forward part ($|\eta| > 2.0$) of the detectors. Without detailed Monte Carlo simulations for the Run III environment and lacking the experience of operating the preshower detectors in Run II, it is difficult to quantify the degredation of preshower performance in Run III. We will assume the preshower detectors continue to be deployed as in Run II. Despite the high occupancy, the basic function of the preshower detectors will remain the same in Run III. Through early energy sampling and precise position measurement, the detector will improve electron identification beyond that provided by the electromagnetic calorimeter and the magnetic tracker, in particular for high p_T electrons.

4 Muon Detectors

Due to their unique properties muons have played an important role in most recent high energy physics discoveries: charm and bottom quarks, W and Z bosons and, most recently, the top quark. Muon decay modes of heavy objects typically have low backgrounds and can be selected using simple trigger algorithms. Muons can be successfully used to tag heavy quark jets (b jets, for example).

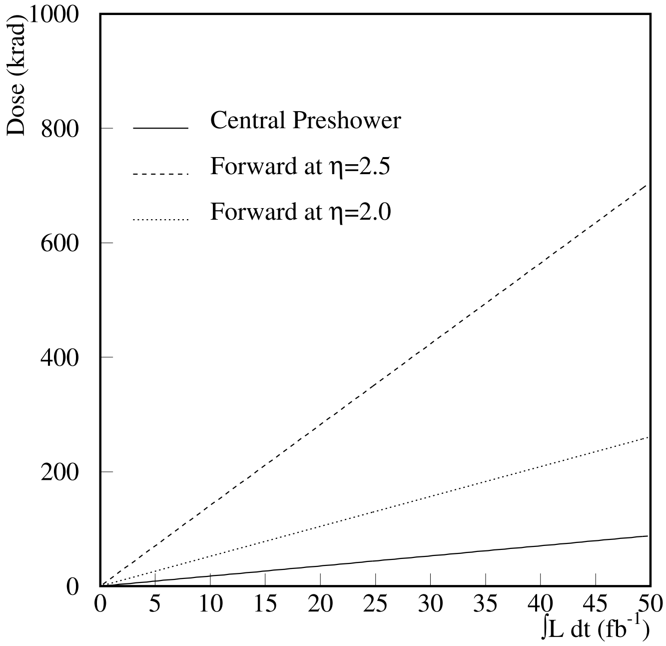

Figure 3: The estimated total radiation dosage in the central preshower detector as functions of integrated luminosity. Also shown are the expected dosage for the forward preshower at $\eta = 2.0$ and 2.5.

At a hadron collider, objects with large mass are typically produced almost at rest in the center of mass system. Detection of their decay products is proportional to the detector solid angle coverage. A hermetic muon system with large rapidity coverage is then an advantage in the search for new objects. Calculations show that a geometric coverage of $|\eta| < 2$ results in 90% acceptance for the decay products of heavy objects [10]. This is why the DØ muon system will have a pseudorapidity coverage to $|\eta| < 2.0$.

Another important feature of the DØ muon system is its thickness, which ranges from 14 (central) to 18 (forward) interaction lengths of material. This drastically reduces hadron punchthrough and other backgrounds. The relatively small decay volume before the calorimeter provides low π/K decay backgrounds. The magnetized toroids give an independent momentum measurement to that of the solenoid which helps with muon triggering and identification.

Below, we will describe DØ muon system design for the first run during Main Injector era in 1999 with luminosity of $2 \times 10^{32}\mathrm{cm}^{-2}\mathrm{s}^{-1}$. We will then define the limits of normal operation of the muon system with increasing luminosity and describe the modifications which are necessary in order to run at luminosity of $1 \times 10^{33}\mathrm{cm}^{-2}\mathrm{s}^{-1}$.

4.1 DØ muon system for Run II

The layout of the DØ muon system for Run II is shown in Figure 4. It consists of central and two forward toroids with average magnetic field of 1.8T. In the central region ($|\eta| < 1.0$) two layers of scintillation trigger counters are used to trigger on muons and reduce cosmic ray backgrounds in the muon samples. Proportional Drift Tubes (PDT) are used to reconstruct muon tracks. They have drift cells with a cross section of 5 cm $\times$ 10 cm and length up to 5 m. The three PDT layers in the muon system are called A, B and C starting from the closest to the interaction region.

In the forward region ($1.0 < |\eta| < 2.0$), there are three layers of scintillation counters with projective tower geometry. Their segmentation is 0.1 in ϕ by 0.1 in η. These counters are used for muon triggering and ϕ track determination. For muon track reconstruction, three layers of Mini Drift Tubes (MDT) are used with a total number of ten detector planes (4A+3B+3C). They have drift cells with 1 cm $\times$ 1 cm cross section and are up to 6 m in length.

To reduce backgrounds from beam jets and interactions with accelerator elements, special shielding (see Fig. 4) will be installed around beam pipe. It consists of soft steel, polyethylene and lead and reduces background fluxes on forward muon detectors up to 50 times with respect to the rates without shielding.

Due to the reduction in beam crossing time from 3.5 μs to 132 ns, all the muon electronics is being rebuilt using a deadtimeless pipeline design. Three levels of triggering will be implemented. At Level 1, raw information about hits in muon detectors is used. At Level 2, special processors run to purify the event sample using detailed information about hits in different muon detectors. Finally, Level 3 is based on an offline type of computer farm with high level algorithms and links between different detector subsystems. Level 3 selects the events to be written to tape.

The muon detector acceptance for η less than 2.0 is around 80% . The losses are mainly due to "no detector" zones under the calorimeter (supports) and between chambers. The momentum resolution of the muon system alone is around 20% and limited by multiple scattering in the iron toroids. Although this is worse than the resolution of the central tracker, it is still useful for muon identification, particularly inside jets. Most of the elements are the same as they were during the first DØ run which began in

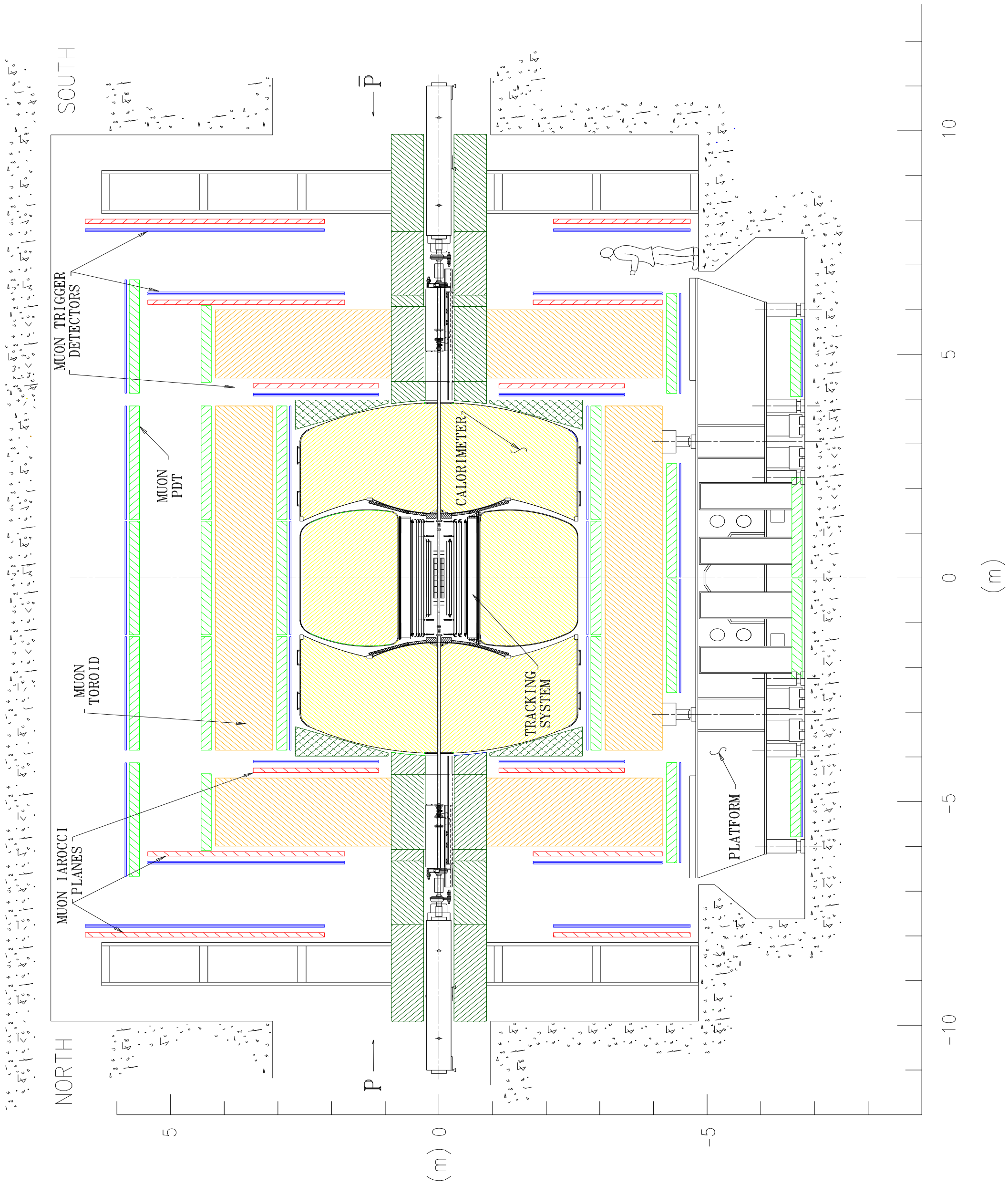

Figure 4: Layout of the DØ detector for Run II.

1992 (see [11]). These include the toroids and central PDTs. New detectors will be added during the 1996-1999 shutdown. The details of the upgrade for Run II are presented in [10].

4.2 Detection of Muons by DØ at TeV33 Luminosity

In the following we summarize the operation of the DØ muon system when the luminosity reaches 1×10^{33} cm^{-2}s^{-1} and determine which elements will start to fail.

The inclusive single muon rate for $|\eta| < 2.0$ is 1 kHz at luminosity of 1×10^{33} cm^{-2}s^{-1}. Most of them are from b-quark decays. The hits in muon detectors from real muons are still negligible in comparison with hits from other sources. The most serious source of hits in muon detectors is remnants of high energy showers leaking through natural holes (for cables, beam pipe, etc.) in the detector. In addition, low energy neutrons will create a "neutron gas" inside the collision hall. These neutrons will interact with nuclei and produce gamma rays which, through photo-electric conversion and Compton scattering, will produce hits in the muon detectors. We have done detailed studies of backgrounds in the DØ detector using Monte Carlo simulations (GEANT, GCALOR, MARS) and results obtained in Run I. The typical flux of charged particles in the central region will be around 2×10^5 particles/m^{2}s at luminosity of 1×10^{33}cm^{-2}s^{-1} (here and below all numbers correspond to Tevatron luminosity of 1×10^{33}cm^{-2}s^{-1}). Based on known particle fluxes [10], we can estimate occupancy of different muon detectors. The occupancy is defined as the probability to find a hit in an event in a single detector cell. For the central system, the PDT occupancy will be around 15%. For the MDT, occupancy will be 0.3% and for scintillation trigger counters occupancy will be around 0.5%. The drastic difference in PDT and MDT occupancy is due to different cell sizes and maximum electron drift times. Due to the unacceptablely high occupancy, the PDTs must be replaced in Run III.

Another serious problem is radiation induced aging of the detectors. The central muon PDTs can handle only around 1mC/cm of anode charge [12]. Although methods of cleaning anode wires have been developed [13], they require a long shutdown in order to clean all wires. From our experience in Run I, we can predict a useful lifetime for the PDTs of about 1 fb^{-1} which is much less than 30fb^{-1} planned for TeV33. For the MDTs, an anode charge of more than 1C/cm (see Figure 5) can be accumulated. This corresponds to integrated luminosity of 100 fb^{-1}, even in the most forward region of the detector where particle fluxes are the highest.

For the scintillation counters, aging of the scintillator and wave-length shifter is not a problem up to 100 krad doses. These detectors will get only about 1 krad at 30 fb^{-1}. After 30 fb^{-1}, phototube gain will decrease by approximately 10% to 20% due to dynode aging. This degradation can simply be corrected by a 40 V increase in cathode voltage.

Accordingly, all the muon detectors, except the PDTs, will be able to run at luminosity of 1×10^{33}cm^{-2}s^{-1}. High PDT occupancies and fast aging require their replacement for the TeV33 era. We propose to replace these chambers with chambers similar to the MDTs. The MDTs can be produced in any preselected length in large quantities and are relatively inexpensive. The new MDT style chambers can be made to be the same mechanical sizes as current PDT chambers, and will simply fit into the existing detector. The typical structure of one MDT layer is shown in Figure 6. The total number of MDT channels needed to replace central PDT is 72,000. In the forward muon system 48,000 MDT cells will be used for Run II. Based on a detailed cost estimate made for Run II, the cost of PDT replacement is around $5M (including electronics). This is the largest part of the DØ muon system upgrade for TeV33. The rest of the system can be used without modification.

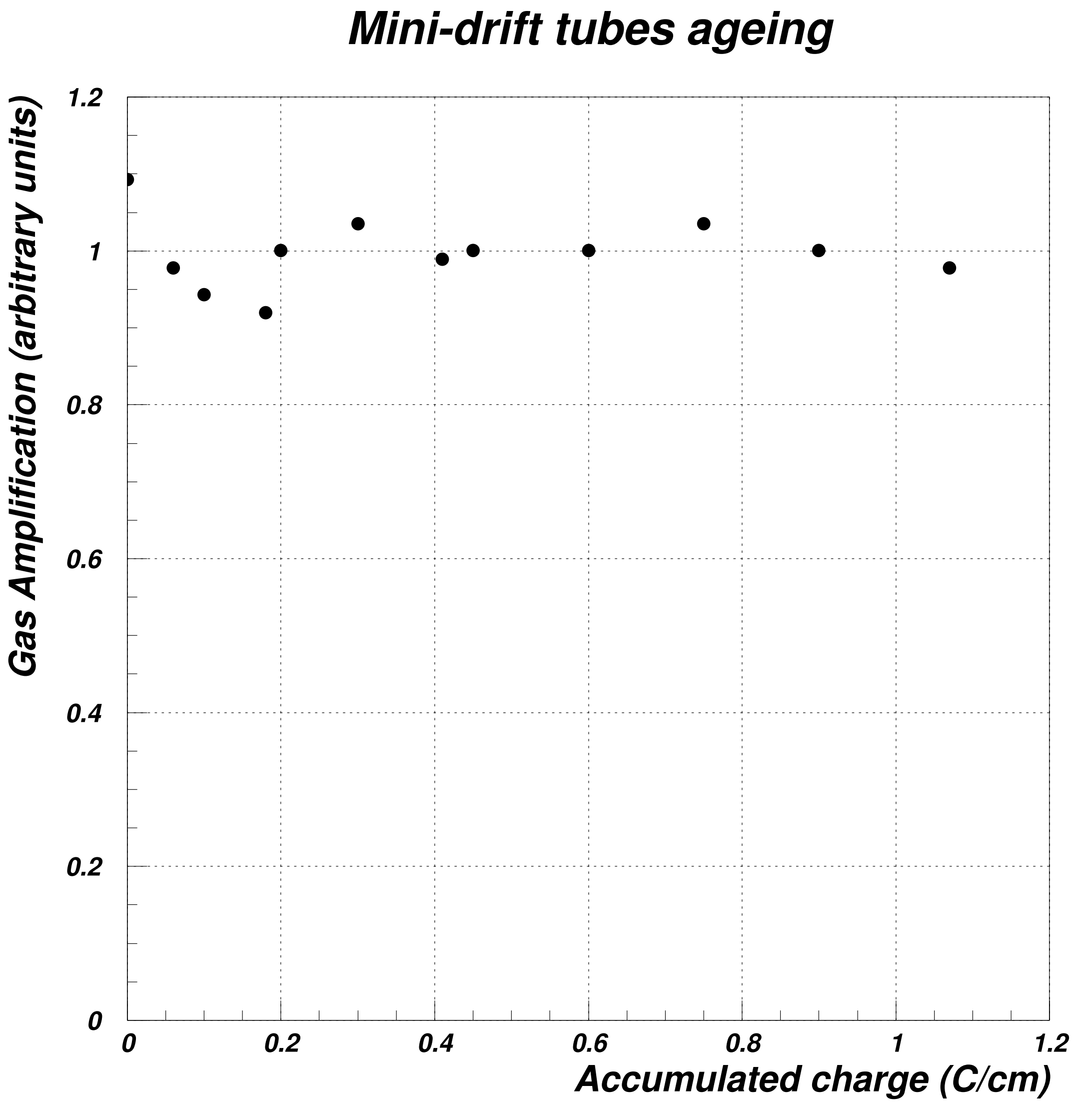

Figure 5: Relative gas gain of MDT vs. accumulated anode charge. Gas mixture of CF_4(90%)+CH_4(10%) was used.

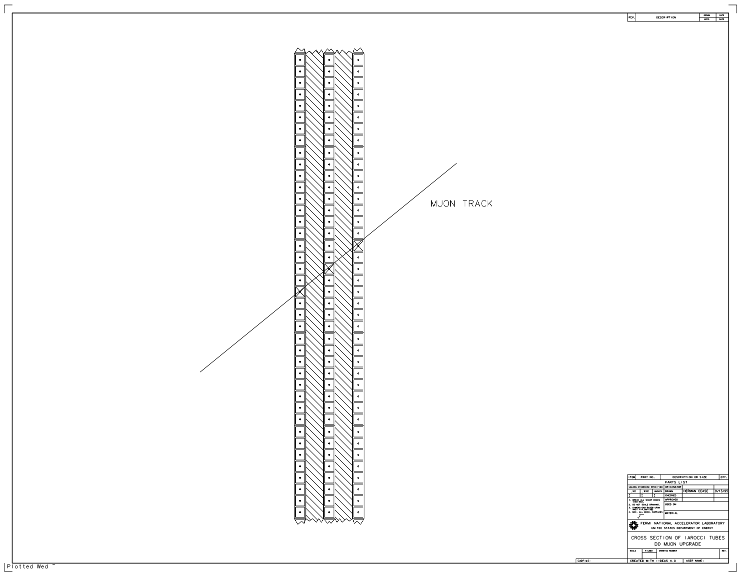

Figure 6: Design of 3-deck MDT chamber.

4.3 Muon Electronics, Trigger and Reconstruction

All muon front-end electronics and trigger system are designed to run at a beam crossing time of 132 ns or larger. Thus we propose that the beam crossing time not be decreased below 132 ns for the TeV33 project to preclude an expensive and time consuming electronics replacement. The MDT electronics for the central PDT replacement will be done exactly as the forward region electronics, saving time and expense in design and commissioning. With "luminosity leveling" (constant luminosity during the store) and filling two out of three abort gaps, the average number of interactions per crossing will remain close to the value planned for Run II at luminosity of $2 \times 10^{32}\text{cm}^{-2}\text{s}^{-1}$. Our studies show that muon trigger rates are a function of the average number of interactions per crossing (not luminosity directly) if the detector latency is less than the beam crossing interval. In this case, the trigger rate estimate performed for Run II [10] will be valid. Taking into account increase in combinatoric rates due to the neutron gas density increase, we estimate the Level 1 single muon trigger rate to be 1–2 kHz. Level 2 and Level 3 triggers will be used to select a clean sample of events with muons. The real muon rate with p_T above 3 GeV/c will be around 100 Hz and can't be written to tape without prescaling. Higher p_T thresholds will be used (real muon rate is approximately 1 Hz for p_T above 10 GeV/c) or more complex triggers (muon+jets, muon+electron, dimuon, etc.) will be used to select interesting events. Reconstruction of muon events with typical detector occupancy below 0.5% will not a problem. In the 1992-1996 Tevatron run, the forward muon system had an occupancy of 5% on average and algorithms to reconstruct muon tracks have been developed. We anticipate high efficiency of muon track reconstruction (above 90%) and propose to use existing software with minor modifications.

4.4 Muon Summary

A large part of the DØ muon system designed for Run II will be able to run at a luminosity of $1 \times 10^{33}\text{cm}^{-2}\text{s}^{-1}$ without modification. We will have to replace the central muon PDT chambers with the MDT chambers of the same design as those used in the forward region for Run II. An early

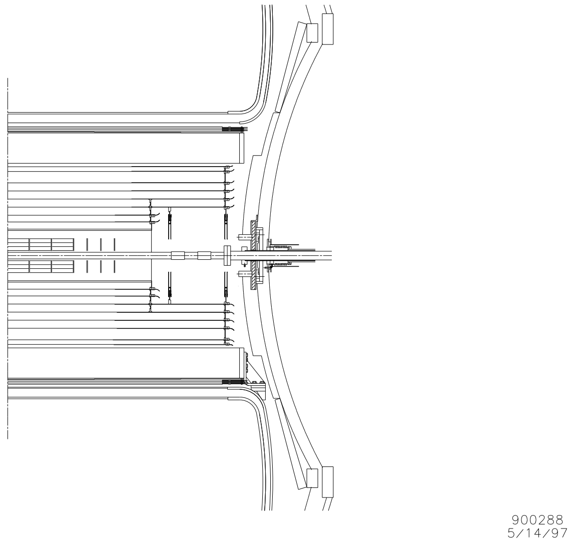

Figure 7: Elevation View of one end of the Central Region of the upgraded DØ Detector. Shown at inner radii are three of the six silicon barrels, containing four layers of detectors each, surrounded by eight superlayers of scintillating fibers. Additionally the are a number of stations of silicon disc detectors covering the forward direction, several of which are intersperced within the barrel region.

decision on the TeV33 project and approval of the detector upgrade will enable us to utilize existing Run II production facilities for the mini-drift tubes and front-end electronics. This replacement will cost around \$5M (in FY96 dollars) including detectors and electronics. The rest of the muon system will be capable of handling luminosity of $1 \times 10^{33}\text{cm}^{-2}\text{s}^{-1}$ and an integrated luminosity of 30 fb^{-1}.

5 Central Tracking

The DØ Tracker consists of a silicon strip vertex tracker (SVT) and a central scintillating fiber tracker (CFT). The tracking devices are situated close to the beam (2.5 cm $\leq r \leq$ 52 cm) and surround the collision region, see Fig. 7. The SVT provides identification and reconstruction of primary event vertices and secondary decay vertices. The CFT provides a Level-1 track trigger with programmable p_T threshold and, in association with the SVT, provides for global track reconstruction and momentum measurement.

The SVT and CFT tracks have a uniform distribution in η and a steeply falling p_T spectrum. The SVT and CFT were originally designed for ten years of operation at a luminosity of $1 \times 10^{32}\text{cm}^{-2}\text{s}^{-1}$. Beam crossings every 132 ns pose no intrinsic difficulty, as signal formation and collection times in these trackers are easily faster than this crossing interval. However, as the luminosity of the Tevatron collider rises above 2×10^{32} $\text{cm}^{-2}\text{s}^{-1}$, the increase in the mean number of collisions per crossing ($\overline{n}$) leads to a rapid degradation of CFT Level-1 track triggering. Extended periods of high luminosity operation pose a problem for detector lifetime for the inner layers of both the SVT and CFT.

5.1 Silicon

In the case of the silicon system as presently designed, the inner two layers will need to be either replaced with a more radiation hard device or removed to larger radii for high luminosity operation.

The increase in bias voltage required for operation renders problematic the current detectors placed at small radii relative to beam. Operation is problematic even with the cooling of the devices. Since radiation exposure falls off as the square of the radial distance from the beam, it is clear that withdrawing the inner silicon layers from 2.5 cm to a position at 4 or 5 cm will lead to a factor of 2.5 to 4 increase in useful detector lifetime. However, this will significantly degrade the impact parameter resolution of the detector. A better proposal is to start an R& D effort to develop a suitable replacement detector. Possible candidates are diamond strips and silicon pixels. The goal would be to develop a radiation hard detector that provides better resolution than the present silicon detector.

5.2 Scintillating Fibers

Fig. 8 shows the mean detected photoelectron signal for a scintillating fiber on the inner barrel of the CFT. The multiclad fiber (830 μm diameter and 1.7 m length) is optically coupled to a clear fiber waveguide of identical diameter and 10 m length, and is read out with a Visual Light Photon Counter VLPC. The minimum detected photoelectron signal occurs for minimum ionizing particles traversing the fiber at normal incidence near the mid-point along the fiber length, which corresponds to the minimum path length. At this location ($\eta \sim 0$), we expect to detect a mean of 11 photoelectrons PE per MIP. A threshold in photoelectron equivalents is set for every channel of the CFT, which establishes the noise rate and efficiency for each. Typically, thresholds are set at 1–1.5 PE, yielding noise rates $< 0.5\%$, and efficiencies $> 99\%$. The efficiency of a fiber-doublet ribbon will also exceed 99% under these conditions.

Higher luminosity operation at TeV33 will modify the detected photoelectron distribution, fiber efficiency, and fiber-doublet ribbon efficiency.

- Radiation damage to the fibers.

The effect of radiation damage is proportional to $r_{\perp}^{-2}$ hence detectors placed at inner radii are most at risk see Fig. 9. In one TeV33 year, we expect an integrated dose of approximately 100 kRad to scintillating fibers situated on the innermost support cylinder ($r = 20$ cm) of the CFT. This corresponds to a factor of two reduction in the optical attenuation length of these fibers, see Fig. 10. Additionally, $\sim$1.5 meter of the clear fiber waveguide will be similarly affected. Together, these effects result in a 33% drop in the detected photoelectron yield at $|\eta| \sim 0$ from fibers placed at $r = 20$ cm, see Fig. 8.

The light loss reduces the tracking efficiency for an inner fiber-doublet layer from a value greater than 99% to approximately 98%. While designed to survive for 10 years of operation in Run II, the existing inner CFT layers would need to be recycled yearly or placed at larger radii for Run III.

- Rate dependence of the VLPC photosensors.

Potential rate dependences of the gain and quantum efficiency of the VLPC photosensors have been studied for 1700 channels of the devices that will be used in Run II. By operating the devices at a temperature of $\sim$ 9K and at a nominal 6.5 V bias, full performance can be maintained at photo-rates well above those expected for either Run II or Run III. Figure 11 displays the efficiency of these devices at 40 MHz. The rate dependence leads to a reduction in detection efficiency per fiber doublet ribbon from 99% to 98% across the full range expected.

- Increased occupancy of the fiber layers.

Tracking detector occupancy is proportional to $\overline{n}$, see Fig. 12. As simulation studies have shown (Fig. 13), ghost clusters in the tracking layers and Level 1 tracking-trigger rates increase as a strong

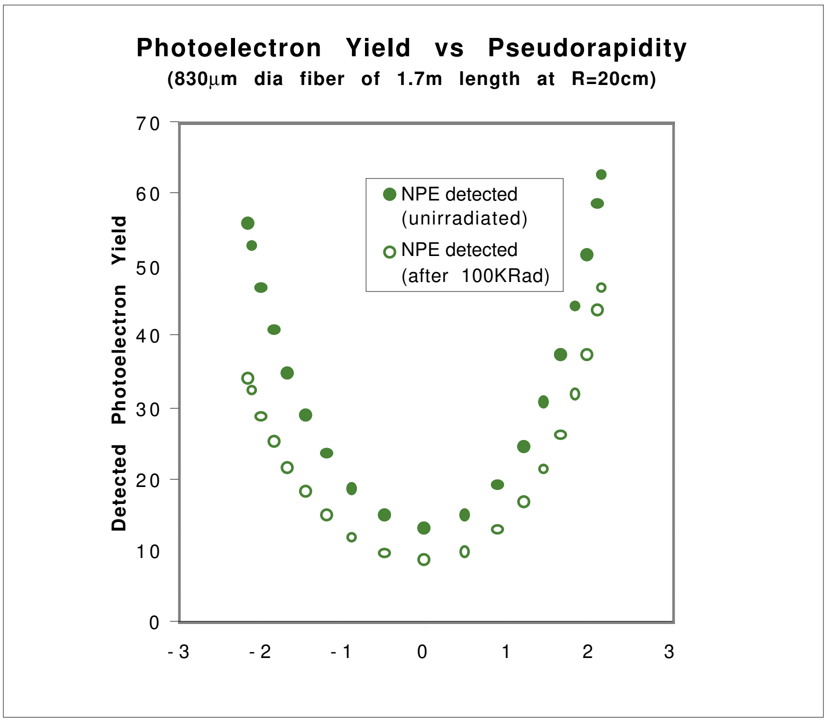

Figure 8: Detected photoelectron signal for the inner layer of the CFT as a function of pseudorapidity, before and after 100 kRad of irradiation. This integrated dose corresponds to 1 TeV33 year.

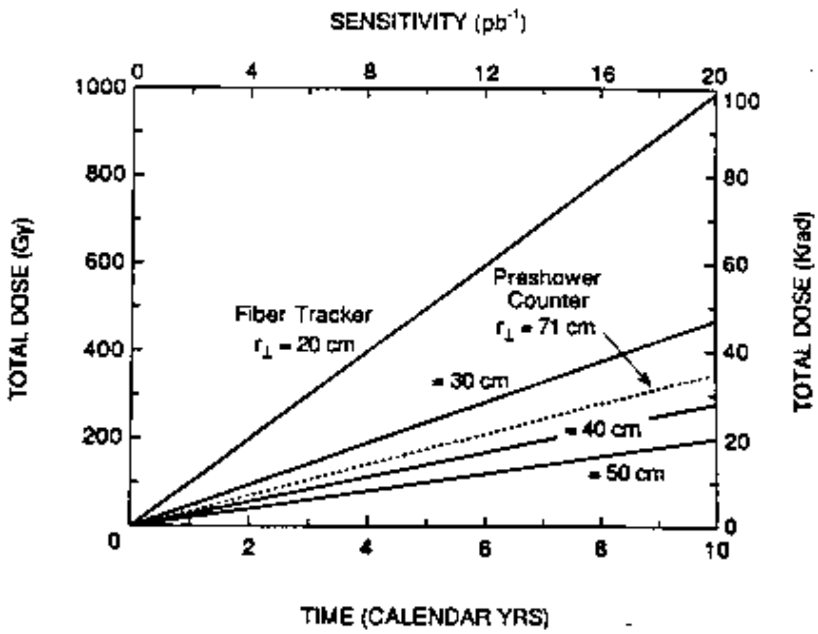

Figure 9: Radiation dose due to charged particle fluence as a function of radial position, in Run II years. (Ten Run II years = one TeV33 year.)

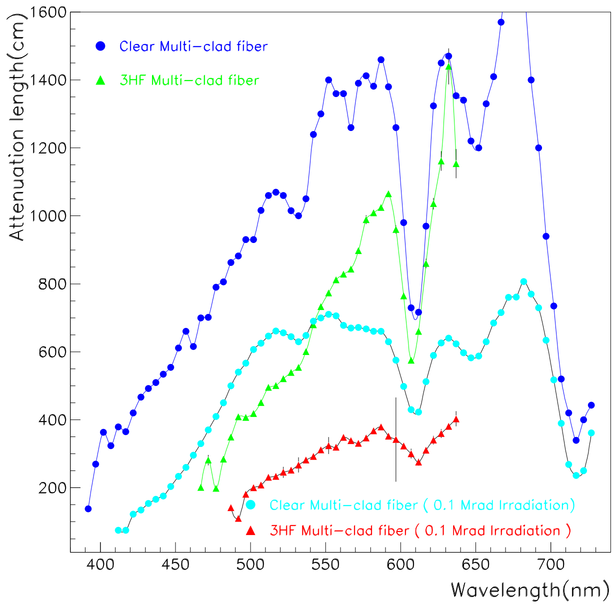

Figure 10: Optical transmission as a function of wavelength for 3HF scintillating fiber and clear waveguide fiber before and after 100 kRad of irradiation.

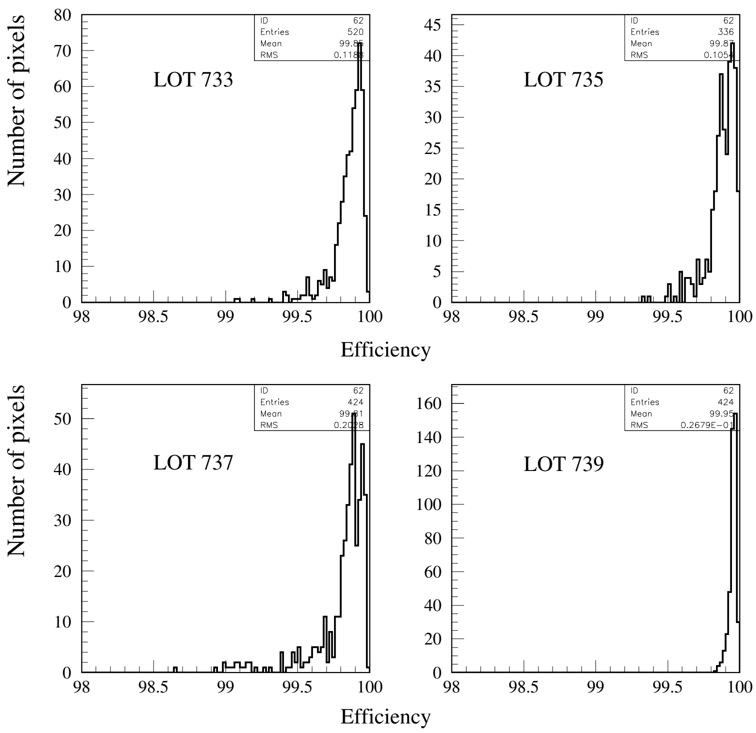

Figure 11: Efficiency of about 1600 channels of VLPCs at an equivalent single photoelectron rate of 40MHz, typical of TeV33 operation at inner tracking radii. Efficiencies greater than 98.5% are indicated.

function (more than linear) of $\overline{n}$. This occurs because the dominant contribution to tracking triggers at a fixed p_T threshold are fakes, accidental alignments of combinations of hits from lower p_T tracks, particularly from jets. To operate within the 10kHz trigger bandwidth available into Level 2, it is essential to maintain a useful level 1 track trigger in combination with calorimeter, preshower, and muon-system triggers. This necessitates keeping $\overline{n}$ as small as possible and also keeping the occupancy per fiber as small as possible. Luminosity leveling can help control $\overline{n}$. Controlling the occupancy per fiber requires either modification or repositioning of the fiber layers.

The occupancy increase presents the greatest challenge to the current CFT design. Potential solutions to the occupancy problem include the following. Using fibers: (1) moving the inner fiber layers outward to larger radii, for example $r \geq 30$ cm, (2) splitting the fibers in the middle (at $\eta = 0$) for the layers at small radii, and (3) reducing the fiber diameter from 830 μm to 500 μm. Alternatively, we could employ other dectection techniques such as coarse pitch (thick strip) silicon detectors for 20 $\leq r \leq$ 30 cm for local tracking and track-triggering. This latter option is discussed in the section on triggering.

5.3 Tracking Baseline for TeV33 and Summary

A robust central tracking system and Level 1 trigger is important for successful operation of DØ under TeV33 conditions. Radiation levels require the repositioning of silicon detectors to greater radial distances or replacement of inner layers with new technologies. Occupany levels may dictate the removal of fiber tracking layers to larger radii or substitution of finer segmentation detectors. A robust Level 1 track trigger necessitates the *in situ* formation of trigger primitives, rather than trigger formation off-detector. A possible TeV33 tracker would include:

- Relocation of the inner silicon microstrip tracker to the radial region 4 cm $\leq r \leq$ 16cm
- Relocation of the inner scintillating fiber tracking layers to larger radii 35 cm $\leq r \leq$ 52 cm
- A "wide strip" silicon tracking and track triggering structures in the intermediate radial region 20 cm $\leq r \leq$ 30 cm
- Removal of silicon disks and repositioning of barrels to close gap left by the disks

Detailed simulation of tracking and triggering in such a system and an active ongoing program of detector R&D are required. For the scintillating fibers this program includes: studies and optimization of smaller diameter scintillating fibers (500 μm diameters), and smaller diameter VLPC pixels (4 x 8 arrays in the same amount of silicon as the current 2 x 4 arrays). For microstrip detectors: evaluation of diamond microstrip detectors, developement of coarse silicon strip detectors, development of local trigger towers based around these technologies. For pixels: R&D on adapting the LHC pixel detectors and readout for DØ.

6 Trigger and Data Acquisition

The average number of interactions per crossing at $\mathcal{L} = 2 \times 10^{33}\mathrm{cm}^{-2}\mathrm{s}^{-1}$ and 108 bunches is 18. Calorimeter based triggers are not very sensitive to the number of minimum bias events in a crossing

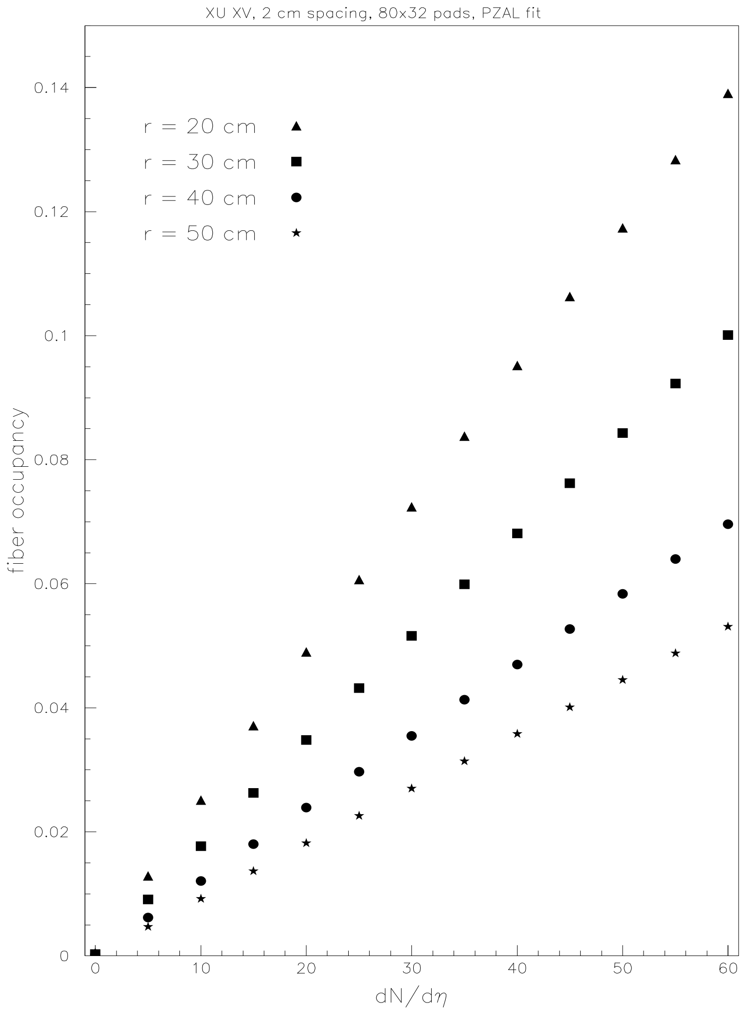

Figure 12: Occupancy as a function of $\overline{n}$ for various tracking radii. Scintillating fibers of 830 μm diameter are assumed. $\overline{n} \geq 6$ (or dN/d$\eta \geq 60$) is typical for TeV33 operation at 132 ns with luminosity leveling.

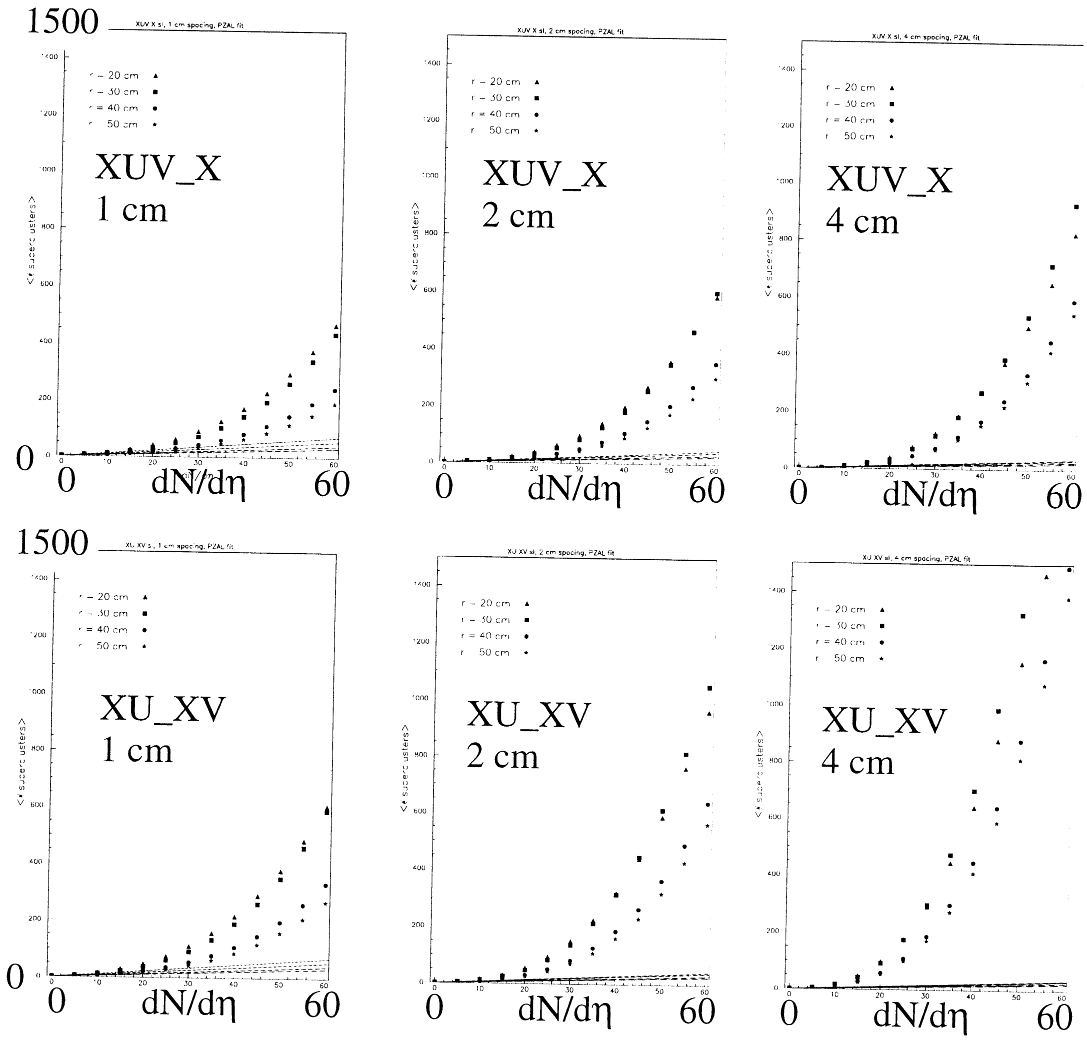

Figure 13: Increase in fake track clusters as a function of event pile-up. A dN/dη of 10 corresponds to an $\overline{n} = 1$; dN/dη of 60 corresponds to an $\overline{n} = 6$, and similar to luminosity-leveled TeV33 operation.

but tracking triggers are very sensitive because of fake tracks. The fiber tracker trigger rejection decreases quadratically with the number of minimum bias events so a factor of 10 increase in luminosity decreases the rejection by a factor of 100. In addition, the number of minimum bias events per crossing are Poisson distributed. One percent of the crossings will have 28 or more events. If one is not careful, tracking triggers will select crossings with large numbers of minimum bias events rather than events of interest.

There appear to be only two solutions to this problem. One is to increase the resolution of the detectors so that the occupancy per channel decreases, and the other is to decrease the intensity per bunch. The latter can be accomplished by increasing the number of RF buckets filled with particles or applying some form of luminosity leveling or a combination of the two. Our preference is to keep as much of the existing detectors as possible so we will concentrate on the latter option. However, it is likely that all of the options will be needed to operate at $\mathcal{L} = 2 \times 10^{33}\mathrm{cm}^{-2}\mathrm{s}^{-1}$.

Filling 2 of the abort gaps presents only a few problems. Each abort gap contains 139 RF buckets. At 132 ns spacing, each of the gaps will hold 19 bunches. If 2 are filled the total charge in the machine is spread over 146 bunches rather than 108 which reduces the number of interactions per crossing from 18 to 13.3. This does have implications for the calorimeter electronics, however.

Luminosity leveling is also possible [14]. At the beginning of a store the low beta is set to roughly half of its maximum possible value. This gives about one half of the maximum possible luminosity. As the luminosity decays, the beta value is decreased at the same rate so that constant luminosity is achieved. This continues until the minimum low beta is reached. After this point the luminosity would decay away just as it did in Run I. Of course, this has never been done before so accelerator R&D is required. There is also some luminosity penalty associated with this; the integrated luminosity over the store is reduced by 10% to 20% compared to one without leveling. However, it reduces the number of interactions per crossing to 6.7 which is only 3.7 times larger than Run II, rather than 10 times larger.

6.1 Run III Trigger Rates

We assume that at TeV33 physics interests will center on high p_T processes. We expect a high p_T trigger rate of 3–4 kHz in Run II. If we implement all of the options mentioned above, the events per crossing increase by a factor of 3.7 so the real trigger rate is approximately increased by this amount. (4 kHz is small compared to the 7 MHz crossing rate). This gives a trigger rate of 11–14 kHz. This is not too far above our Run II design goal of 10 kHz. This has no safety factor so it might be reasonable to put in a factor of 1.5 or so which would raise the peak rate to about 20 kHz which is twice the Run II design.

There are two ways to treat the increased Level 1 accept rate. We can rebuild all the tracking and calorimeter electronics and the Level 2 and Level 3 systems to accept 20 kHz (replace the SVX II chips, etc.) or we can move some of the rejection power in the Level 2 processors to Level 1 so that we can fit all the high p_T physics into the existing 10 kHz bandwidth. The latter appears to be the best choice although some more study is needed. The impact of this on each system is described below.

6.1.1 Muon Trigger

The Level 1 muon trigger for TeV33 will be similar to that used in Run II. The Run II Level 1 muon trigger searches for muons locally in octants in geographic region. Within each octant, one muon trigger

Table 1: Muon trigger rates for different trigger conditions at luminosity of 2×10^{33} cm-2 s-1 for two and eight interaction Monte Carlo samples. Each sample has been normalized to 40 mb. Note the single muon rate (transverse momentum > 8 GeV/c and $|\eta| < 1.5$) from $b\bar{b}$ production alone is roughly 100 Hz at TeV33 luminosities.

Muon Trigger Condition	2 interaction	8 interaction	increase
CFT alone (8 GeV/c)	199 kHz	58600 kHz	294
CFT·APHI	0.7 kHz	1986 kHz	2837
CFT·central scintillator	0.09 kHz	4 kHz	44
CFT·pixel scintillator	0.02 kHz	0.5 kHz	2.5
PDT AB *OR* AC	13 kHz	4 kHz	0.3
MDT AB *OR* AC	26 kHz	350 kHz	13

card uses combinatorial logic to match tracks from the CFT with either central or forward scintillation counters. The 25 ns gate used with the scintillation counters provides a powerful means of rejecting particles associated with showers originating in beam line elements or detector edges. A second muon trigger card searches for muons using wire hit information from central or forward tracking detectors (MDT's). Wire hits are confirmed by coincidence with the corresponding scintillation counters. Because the MDT's have three or four decks in each layer, "stubs" or centroids can be formed. The angle of these "stubs" provides additional rejection of background not associated with the primary collisions. The octant trigger decisions for each region are collected by a muon trigger crate manager which forms trigger decision bits for that region. Typically, a muon trigger is defined by the AND of the triggers found using the CFT and muon scintillator with those found using muon chamber hit information. Regional trigger decisions from the muon trigger crate managers are sent to the muon trigger manager which forms a global muon trigger decision which is sent to the trigger framework for inclusion in the global physics trigger decision. One method of testing the above trigger logic has been to use ISAJET two jet events which have been fully simulated in the Run II detector using GEANT. Fortran routines containing the trigger logic are used to find the pass rate of multiple interaction events. The trigger rate for one high transverse momentum muon (≥ 8 GeV/c) in the pseudorapidity region $|\eta| \leq 1.5$ for a luminosity of 2×10^{32} cm^{-2} s^{-1} with 132 ns bunch spacing is found to be approximately 500 Hz. This number is dominated by the statistics in the single interaction Monte Carlo files where we have passed one event to calculate an upper limit for the rate. The error on the estimated trigger rate is likely at least a factor of three times the rate due to uncertainties as to how well our ISAJET/GEANT simulation reflects real data and Monte Carlo statistics. At $\mathcal{L} = 2 \times 10^{32}$ cm^{-2} s^{-1}, simple scaling gives a Level 1 muon trigger rate of 5 kHz. As an aside, the single muon rate (transverse momentum ≥ 8 GeV/c and $|\eta| \leq 1.5$) from $b\bar{b}$ production alone is roughly 100 Hz at TeV33 luminosities. Five kHz is then one measure of the estimated muon trigger rate at TeV33. One criticism of the 5 kHz number is that we have not taken multiple interactions per crossing into account. This is obscured by the single interaction files rate as mentioned above. Alternatively, we can use two and eight interaction files separately to make an estimate. The average number of interactions per crossing for Run II is approximately two while with abort gap filling and luminosity leveling the corresponding number at TeV33 is seven. Comparison of muon trigger rates using two and eight interaction Monte Carlo data gives some insight on the how the rates might vary as a function of the average number of interactions per crossing. The fluctuations are representative of our Monte Carlo statistics as well as some uncertainty about the reliability of the eight interaction Monte Carlo set. The results are summarized in Table 1.

One conclusion is that the muon toroid iron provides some measure of protection against the increasing average number of interactions per crossing. Whereas the CFT rate alone increases by a couple of orders of magnitude from two to eight interactions per crossing, those triggers which use muon elements outside the iron toroid increase by roughly a factor of ten. Based on the two and eight interaction Monte Carlo samples alone we would expect muon trigger rates of 100 Hz and 1 kHz. Both are smaller than our 5 kHz estimate (which, to repeat, is dominated by our upper limit for the single interaction files).

The estimated Level 1 muon trigger rate at TeV33 using the Run 2 trigger hardware is 5 kHz. The uncertainty of this number is large, reflecting uncertainties in our modeling accuracy and the poor Monte Carlo statistics we presently have available.

Many Level 2 triggers are being moved to Level 1 for Run II. It is not easy to come up with ideas to reduce this rate. One is to tighten the time cuts on both the scintillator and the wire chambers. Note that these studies are in their very early stages so they are based on very low statistics. The rate could change quite a lot with a more detailed study. Improved tracking triggers could also help.

6.1.2 Calorimeter Trigger

The present calorimeter Level 1 trigger forms towers that are 0.2 by 0.2 in $\eta - \phi$ space. Each tower is summed in depth to give an EM and a Hadron signal. These signals are available to the trigger framework. In addition, signals from 4×8 $(\eta \times \phi)$ trigger towers are summed to form "large tile" signals which are used to search for jets. There are 4 EM threshold reference sets, 4 Jet (EM+HAD) threshold reference sets, and 8 large tile reference sets. Each reference set consists of energy threshold values for each tower. Finally, several global quantities are summed over the entire calorimeter and compared to reference set values. These include the vector sum of momentum (used for missing E_T triggers) and scalar EM E_T and scalar Jet E_T. The only changes anticipated for Run II are providion for direct readout to the DAQ system and to provide a history of the previous 25 crossings.

Increasing the calorimeter trigger rejection requires an entirely new Level 1 trigger system. This system would move the isolation cut for EM jets to Level 1. It would improve the hadron part of Level 1 by allowing a more flexible combination of towers than is provided by the large tiles. That is, one could have a moving window which would search for isolated jets rather than large fixed tiles. It would provide the ϕ of the trigger so that there could be a ϕ match between the tracker, preshower and calorimeter. Putting the isolation cut at Level 1 should easily get a factor of 2 to 3 for electrons. It is not known if the changes to the hadron trigger would give the additional rejection that is required. But if they do not, one can simply increase the prescale factors for these triggers.

It is estimated that the design, construction and installation would take at least 2.5 years and cost \$1.5M. This upgrade would allow us to implement some other useful features such as digital filtering of the input signals to get rid of some of the pile up effects from adjacent crossings.

6.1.3 Tracking Trigger

The Level 1 tracking trigger for Run II is formed by the logical AND of hits from the 8 axial layers of the scintillating fiber tracker. Monte Carlo studies show that the probability of finding a fake track is a strong (more than linear) function of the number of tracks in the detector. The only known solution for TeV33 is to increase the resolution of the trigger elements either by using more layers of (possibly smaller) fibers or by adding some sort of pixel device.

We have looked at the possibility of rearranging the existing fiber detector while keeping the number of detector channels constant. We studied the affect of putting additional layers of 1 mm or 0.5 mm fibers in the region between 40 and 55 cm radius. Figures 14 to 16 show the rejection factor as a function of number of layers for various road sizes for 108 bunches at $\mathcal{L} = 1 \times 10^{33}\text{cm}^{-2}\text{s}^{-1}$ and $\mathcal{L} = 2 \times 10^{33}\text{cm}^{-2}\text{s}^{-1}$, and for 146 bunches at $\mathcal{L} = 1 \times 10^{33}\text{cm}^{-2}\text{s}^{-1}$. There is no luminosity leveling. The revolution frequency is 5 MHz so a rejection factor of 1000 is needed to get to 5 kHz (500 at 2×10^{33}). This is also plotted on the figure. Note that there are no stand alone tracking triggers so the stand alone rate does not have to be below 5kHz. However, we think that a Level 1 accept rate for the tracker of less than 10 kHz is needed because of bandwidth limitations and fakes in other detectors. This has not been studied in detail.

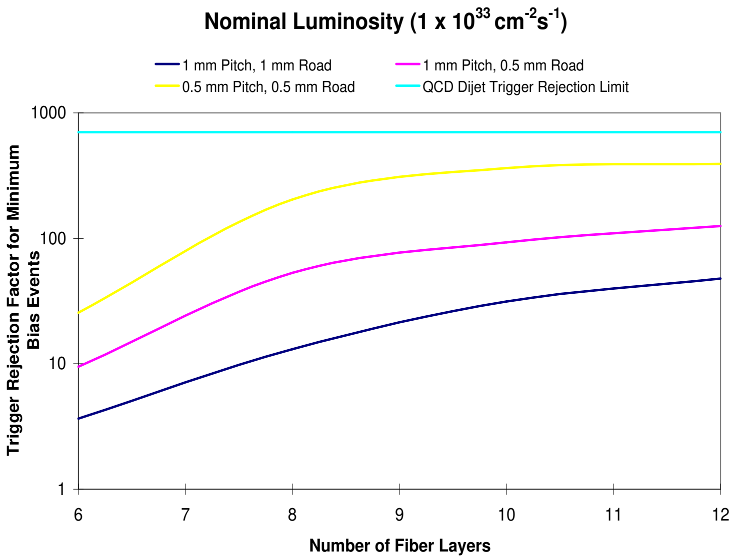

Figure 14: Tracking trigger rejection at $\mathcal{L} = 1 \times 10^{33}\text{cm}^{-2}\text{s}^{-1}$

There is no solution that gets to 5 kHz even with luminosity leveling (the 146 bunch $\mathcal{L} = 1 \times 10^{33}\text{cm}^{-2}\text{s}^{-1}$ plot is equal to $\mathcal{L} = 2 \times 10^{33}\text{cm}^{-2}\text{s}^{-1}$ with luminosity leveling). The best that we can do is a trigger rate of 7 kHz with 9 fiber layers. This may be adequate. However, it does eliminate most of the stereo layers which are needed for off-line reconstruction. Thus, additional detectors or more VLPC channels are needed.

A second possibility is to replace the inner 3 or 4 fiber tracking layers with large pitch silicon detectors. These devices would be built as rectangular pixels and assembled into towers. The device consists of 4 layers of silicon at radii of 20, 22, 30 and 32 cm arranged into 40 towers in ϕ by 40 towers in z. The detectors are wedge shaped in the ϕ direction which is also the pitch direction of the silicon. Thus, the pitch varies from 245 to 392 microns. Each strip (z direction) is 1 cm long. The readout

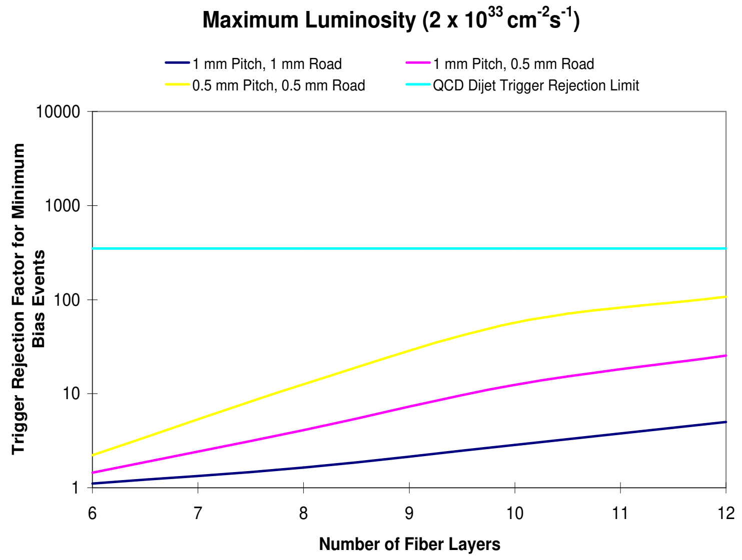

Figure 15: Tracking trigger rejection at $\mathcal{L} = 2 \times 10^{33}\mathrm{cm}^{-2}\mathrm{s}^{-1}$

is by an SVX type of chip with a trigger pick off mounted directly on the detector. The device is constructed as a series of towers inserted into a egg-crate like frame. We have assumed 128 channels in ϕ and 5 pixels in z for each module so the tower is approximately 5 cm square at the top. The trigger is formed by routing the signals from the inner layers to the outer layer via thin Kapton cables. The fourth (outer) layer is also connected by small Kapton cables to each of its four adjoining neighbors. Connection to the diagonal neighbors is possible but it is not thought to be necessary. The fourth layer has a large FPGA chip in addition to the SVX chips so it can form the trigger locally. Timing and trigger information are sent to the module over fiber optic cables. Readout is also over fiber.

There are 40 of these modules in ϕ and 40 in z for a total of 1600 modules. Each module is built in a jig and then tested modules are inserted into the frame. This should allow reasonably easy repair provided that the assembly could be removed from the center of the fiber tracker. There are about 5 million channels in this device which is a factor of 500 more than the Run II fiber trigger that it replaces. One would expect that the occupancies would be reduced by roughly the same amount.

A Monte Carlo study of this detector has been done using the DTUJET generator. This generator produces about 1 high p_T particle per thousand events so we are looking for rejection rates of approximately 1000. For $\mathcal{L} = 1 \times 10^{33}\mathrm{cm}^{-2}\mathrm{s}^{-1}$, we get an acceptance for 10 GeV/c tracks of .09% which is very close to the actual number of high p_T events in the sample. Thus, this trigger can work without any other devices. It would be fairly straightforward to connect this to the fiber tracker in the same way as is done for the muons. Both the intermediate silicon and the fiber tracker would find tracks

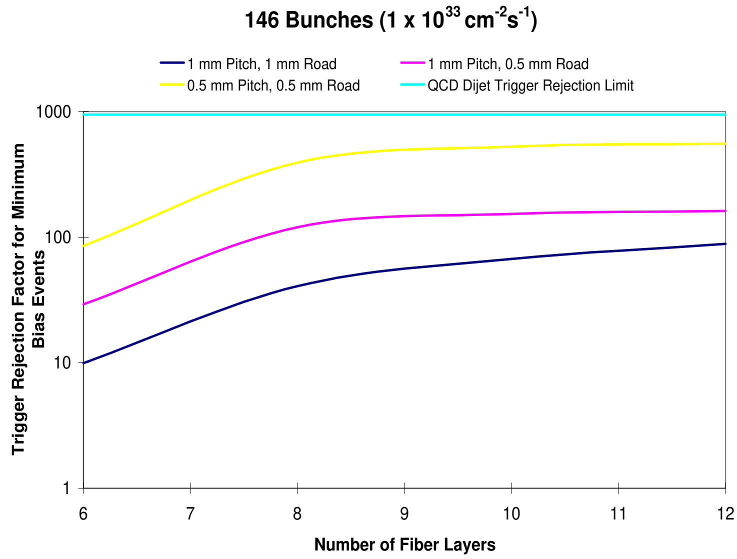

Figure 16: Tracking trigger rejection at $\mathcal{L} = 1 \times 10^{33}\mathrm{cm}^{-2}\mathrm{s}^{-1}$ and 146 bunches

independently and would then be matched together to confirm the tracks.

An intermediate silicon detector would be very powerful for a silicon level 2 trigger. The z segmentation should allow one to easily pick out the event of interest and also to select which of the fiber barrels to read out. This gives an effective segmentation of 6 in z which should help in reducing the background.

This trigger method could also be used for a silicon pixel detector that could replace the inner silicon strip layers. The technical difficulty is that the silicon system would be much smaller so that all devices would be a factor of 5 to 10 smaller. This makes it difficult to fabricate cables connections. Note that the Monte Carlo results for the intermediate silicon detector are also valid for inner layer silicon pixels. The silicon pixels are about a factor of 6 or so smaller than the intermediate silicon detector but they are also about a factor of 6 closer to the beam.

For either type of pixel, the important concept is the idea of local trigger generation. If one takes all of the signals off to some large box, the distribution of information to all the parties that need it becomes a nearly impossible task. In some sense, the data is first randomized on a series of cables and then reordered - a hard task indeed. In this scheme, trigger information is processed where it is gathered and only modules that have a trigger would send out anything. Of course, once a valid Level 1 accept has occurred, all the towers would be read out for Level 2 and Level 3 processing.

7 Conclusions

The physics that can be done with 30 fb^{-1} of data at the Tevatron is compelling, although we have not discussed it in detail here. The DØ detector should perform well in the TeV33 environment with some upgrades. The calorimeter and central preshower detector should perform well without changes. The large $|\eta|$ performance of the forward preshower is likely to suffer from accumulated radiation dose. The central muon chambers will have to be replaced, most likely with the same chambers that will be used in the forward muon system in Run II. This change is straightforward, but will require substantial effort. Central tracking and the trigger will require the most significant changes. A number of plausible plans exist for the upgrades and R&D will be required to decide which is best. Luminosity levelling would help keep the scope of the upgrades reasonable, and would allow them to be done within the desired time and budget.

References

[1] *Future Electroweak Physics at the Fermilab Tevatron: Report of the TeV2000 Study Group*, D. Amidei and R. Brock, editors, Fermilab-Pub-96/082, pp. 220-221.

[2] Ibid., pp. 65-73.

[3] P. Nemethy and A. Mincer, "Pileup Effects on W Mass Measurement," DØ Note 1398 and "Original Electronics versus Upgrade Electronics: Comparison of Pileup at Full Luminosity," DØ Note 1642.

[4] A. Kotwal, "Effects of Multiple Interactions and Pileup on the W Mass Measurement in the Electron Channel in DØ in Run II and TeV33," Fermilab-Conf-97/011-E, *Proceedings of the 1996 DPF Snowmass Summer Study.*

[5] H. Piekarz, " On the Possibility of Speeding-up the Time Response of the DØ Calorimeter," *Proceedings of the 1996 DPF Snowmass Summer Study.*

[6] M. Adams et al., "Design Report of the Central Preshower Detector for the DØ Upgrade," DØNote 3014.

[7] DØ Collaboration, "The DØ Upgrade: Forward Preshower, Muon System and Level 2 Trigger," DØ Note 2894.

[8] M. Adams et al., Nucl. Instrum. and Meth. **A366**, 263 (1995);
M. Adams et al., Nucl. Instrum. and Meth. **A378**, 131 (1996).

[9] S. Margulies and M. Chung, "Estimation of Radiation Doses in the DØ Upgrade Scintillating-Fiber Tracker and Central Preshower Counter," DØNote 2394.

[10] R. Jayanti et al., "The DØ Muon System Upgrade," DØ Note 2780.

[11] S. Abachi et al., Nucl. Instr. and Meth. **A338**, 185 (1994).

[12] J.M. Butler, "DØ Muon Chamber Pulse Heights," DØ Note 2319.

[13] T. Marshall et al., "Crud Removal from Muon Drift Chamber Wires Using "zap" Cleaning," DØ Note 2556.

[14] G. Jackson, luminosity leveling ref, *Proceedings of the 1996 DPF Snowmass Summer Study.*